Simulation of Cyclically Loaded Concrete Structures Based on the Finite-Element Method

Dan Palermo[1] and Frank J. Vecchio[2]

Abstract: The finite-element method for simulating the nonlinear behavior of reinforced concrete structures has progressed to the point where it is close to being a practical everyday tool for design engineers. Further advancements have made the analysis of arbitrary loading conditions, including reverse cyclic loading or earthquake-type loading, feasible. Recent criticism has questioned the practicality, reliability, and robustness of the finite-element method due to perceived complexities involved in developing the model and interpreting the results. A series of analyses are presented on reinforced concrete structural walls of varying height-to-width ratio, varying wall cross section, and varying levels of reverse cyclic loading to demonstrate that the finite-element procedure is capable of providing quick and reliable simulations, while employing simple modeling techniques. The modeling herein utilizes low-powered rectangular membrane elements, and material properties are smeared within the elements. Behavioral aspects such as ultimate strength, displacements, postpeak ductility, energy dissipation, and failure mechanisms are well simulated.

DOI: 10.1061/(ASCE)0733-9445(2007)133:5(728)

CE Database subject headings: Nonlinear analysis; Finite element method; Hysteresis; Cyclic loads; Shear walls; Concrete structures; Simulation.

Introduction

The finite-element (FE) method was first introduced to practicing engineers in the aircraft industry in the 1950s. The term "finite element," however, was not adopted until 1960 (Clough 1980). By the early 1960s the validity of the FE method was recognized and the method was expanded beyond structural applications (Cook 1995). General purpose FE software began to appear during the 1970s, and by the 1980s software was available for microcomputers. Occurring during the same period were significant advancements in computing technology, greatly expanding the size of analyses that could be considered and greatly reducing the time required for solutions. Some estimates indicate that by the mid-1990s some 40,000 papers and books on the FE method and its application were published.

Likewise, procedures for nonlinear finite-element analysis of reinforced concrete structures have developed where they can be regularly incorporated in design and analysis applications. Various approaches have been taken, differing in such aspects as stiffness formulation (tangent versus secant stiffness), constitutive modeling (plasticity-based, fracture mechanics, and nonlinear elastic models), element preference, and crack models (rotating versus fixed, and discrete versus smeared). Researchers working in each of these areas have demonstrated varying degrees of success in simulating the response of reinforced concrete structures. These efforts are well-documented by the American Society of Civil Engineers (ASCE 2001).

Procedures that provide adequate simulations of behavior under arbitrary loading conditions, including reverse cyclic loading, are less common than models applicable to monotonic loading. Okamura and Maekawa (1991), Sittipunt and Wood (1995), Foster and Marti (2003), and Palermo and Vecchio (2004) among others (ASCE 2001) have documented models that have demonstrated reasonable agreement with experimental results.

Despite the extensive and exhaustive research conducted in the area of FE analysis of reinforced concrete, significantly differing viewpoints remain regarding its effectiveness. Some researchers believe that finite-element models can provide a refined and detailed definition of the local response, while others contend that their efficiency, practicality, and robustness are questionable due to perceived complexities involved in developing the model and interpreting the results (Orakcal et al. 2004).

Research Significance

The need to demonstrate that the finite-element method can be an effective and simple tool, while providing quick and reliable solutions, has been brought to the fore by recent criticism. Further, there is a need to provide design office engineers with appropriate methods and models to simulate the response of structural walls.

This paper will present nonlinear finite-element analyses using a well-established analysis method. The emphasis is on the simplest form of modeling available for continuum FE analysis, utilizing low-powered elements and smearing of the material properties. It will be demonstrated that accurate simulations can be obtained, including aspects relating to ultimate strength, dis-

[1]Assistant Professor, Dept. of Civil Engineering, Univ. of Ottawa, 161 Louis Pasteur St., Ottawa ON, Canada K1N 6N5. E-mail: palermo@eng.uottawa.ca

[2]Professor, Dept. of Civil Engineering, Univ. of Toronto, 35 St. George St., Toronto ON, Canada M5S 1A4.

Note. Associate Editor: Dat Duthinh. Discussion open until October 1, 2007. Separate discussions must be submitted for individual papers. To extend the closing date by one month, a written request must be filed with the ASCE Managing Editor. The manuscript for this paper was submitted for review and possible publication on April 12, 2005; approved on September 7, 2006. This paper is part of the ***Journal of Structural Engineering***, Vol. 133, No. 5, May 1, 2007. ©ASCE, ISSN 0733-9445/2007/5-728–738/$25.00.

placements, postpeak ductility, energy dissipation, and failure mechanisms, while maintaining simplicity in the finite-element models. The analyses undertaken include walls subjected to reverse cyclic loading conditions, consisting of varying height-to-width ratio and varying cross section, to address the wide range of shear walls integrated as primary lateral-force-resisting elements.

Finite-Element Modeling

Conceptual Model

Pioneers (Darwin and Pecknold 1976) in the area of finite-element modeling for reverse cyclic loading stated that improved constitutive models for engineering materials were needed to further progress the understanding of structural behavior. For this study, analyses were undertaken using the program VecTor2 (Vecchio 1989), a two-dimensional nonlinear finite-element program for reinforced concrete membrane elements based on the modified compression field theory (MCFT) (Vecchio and Collins 1986). The program was developed with the philosophy of utilizing simple modeling techniques, while concentrating on developing improved constitutive models for concrete and reinforcement. The MCFT, in its implementation into the finite-element routine, has demonstrated success at simulating the behavior of a diverse range of reinforced concrete members, including shear panels, shear-critical beams, shear walls subjected to monotonic and cyclic loading, and rehabilitated or repaired concrete structures. In addition, analyses can be conducted based on the disturbed stress field model (DSFM) (Vecchio 2000). The DSFM is a refinement of the MCFT and explicitly includes calculation of crack shear slip deformations, which eliminates the crack shear check required by the MCFT: a concept least understood by others in their implementation of the MCFT. Further, the inclusion of crack shear slip deformations leads to decoupling of the principal stress field from the principal strain field. Therefore, the principal stress and strain fields are no longer required to be coincident as assumed in the MCFT. The DSFM generally provides a better estimate of strains in the reinforcement, by calculating lower strains in the longitudinal reinforcement and higher strains in the transverse reinforcement. This leads to a better redistribution of stresses in the element. However, a comprehensive evaluation of the MCFT and DSFM (Vecchio et al. 2001) has shown that there is a marginal difference in the calculated monotonic response of shear walls when comparing the MCFT and the DSFM. Further studies also demonstrated little difference for walls subjected to reverse cyclic loading. The DSFM is likely to demonstrate improved performance in situations where there is little to no reinforcement in the transverse direction. In most practical situations, shear walls contain above minimum levels of orthogonal reinforcement and the difference in response between the MFCT and DSFM is likely to be negligible. For this study the analyses are based on the MCFT.

Further advancements in the program have led to the consideration of bond slip between the concrete and the reinforcement (Wong and Vecchio 2003), bar buckling, dowel action of the reinforcement, and loading history. The latter allows analysis of reinforced concrete subjected to arbitrary loading, including reverse cyclic loading (Vecchio 1999), and analysis of repaired or rehabilitated concrete structures (Vecchio and Bucci 1999).

Constitutive Models

For the engineering analyst, the FE method presents significant challenges, which can significantly affect the simulated response. These include the choice of the constitutive material models, the model development, and the material properties.

Modern software typically provides extensive lists of constitutive models for concrete and reinforcement. The intent herein is to simplify the selection process by adhering to default material models, avoiding exhaustive parametric studies. In this study, the VecTor2 default models were used. The only exceptions were the base curve for concrete in compression and the hysteretic model for concrete. The selection of the base curve was significant considering the concrete strength varied from 21.7 to 53.6 MPa for the walls under investigation. Further, a majority of walls experienced concrete crushing.

For concrete compressive strength up to 45 MPa, the Popovics normal-strength model was selected as the base curve. The only exceptions were Walls DP1 and B6 which had strengths of 21.7 and 21.8 MPa, respectively. Optimal results were obtained by using the Smith-Young base curve. For high-strength concrete (strength greater than 45 MPa), which exhibits a stiffer prepeak response and sudden strength decay in the postpeak region, the Popovics high-strength model was chosen. From this study it generally appears that the Popovics normal-strength model is applicable to concrete ranging from 22 to 45 MPa. The Popovics high-strength model is applicable to higher concrete strengths and for concrete below 22 MPa, the Smith-Young curve provides substantial agreement. The one exception was B8 which had a compressive strength of 41.2 MPa. In this case Popovics high-strength curve provided substantial agreement and accurately simulated the onset of failure.

The program default material models were used to capture other relevant features. Compression softening was modeled by Vecchio's 1992-A model (Vecchio and Collins 1993), which accounts for the reduction in compressive strength and stiffness due to coexisting transverse cracking and tensile straining. This model was selected as it considers the softening of both strength and strain. Tension stiffening effects were modeled using the modified Bentz model (Vecchio 2000). It accounts for the tensile stresses that exist in concrete between cracks due to the bond action between the reinforcement and the concrete. This model was specifically formulated to account for the bond characteristics of the reinforcement, and therefore, the influence extends into surrounding elements that do not contain any reinforcement. Tension softening which accounts for the presence of postcracking tensile stresses in plain concrete was modeled with a linear descending branch after cracking. It addresses situations where an element has little to no reinforcement and still contributes to the strength and ductility of the structure. (The tensile postcracking strength of concrete is determined from the maximum of tension stiffening and tension softening.) The dilation of concrete, which accounts for the lateral expansion of concrete due to internal microcracking and increases as the compressive stresses increase, was modeled by a variable Poisson's ratio based on work conducted by Kupfer (Vecchio 1992). The lateral expansion may account for a significant portion of the total strains in the principal tensile direction. If these strains are incorrectly attributed to strains due to stress, an overestimation of the compression softening effect occurs. The effect of lateral expansion was expanded to the out-of-plane direction, even though the MCFT was formulated for plane stress. The presence of out-of-plane reinforcement confines the lateral expansion giving rise to triaxial stress conditions, resulting in

strength enhancement to the concrete in compression. The default model is the Kupfer-Richart model (Vecchio 1992). The cracking strength of concrete was determined from the Mohr-Coulomb stress model. It calculates the cracking stress of concrete which can be different from the concrete tensile strength due to coexisting transverse compressive stresses. Analyses conducted with the MCFT require a crack shear check to ensure that the shear stresses on a cracked surface do not exceed a maximum allowable corresponding to sliding shear failure. The Vecchio-Collins model is used to calculate the maximum shear stress permitted at a crack (Vecchio and Collins 1986). An additional consideration at a crack is the width of a crack and its implication on the compressive strength. This check serves to reduce the compressive stresses when crack widths exceed a specified limit. In the analyses the limit was based on 20% of the aggregate size. The default hysteretic behavior of concrete is based on work conducted by Vecchio (1999). However, for the analyses herein, the model proposed by Palermo and Vecchio (2003) was selected. Studies of the two models (Palermo and Vecchio 2002a) indicate that there is a marginal difference in the overall behavior of walls experiencing flexural dominant behavior. Some differences were noted for walls controlled by shear crushing of the concrete. The model by Palermo and Vecchio is an improvement from the original; it accounts for stiffness and strength degradation of the reloading branches, nonlinear unloading, increased energy dissipation in the hysteretic response of concrete in compression and tension, and specifically accounts for partial unloading and partial reloading. The reinforcement hysteretic behavior follows Seckin's model (Vecchio 1999), which includes the effects of strain hardening and accounts for the Bauschinger effect. Additional details of each of the models can be obtained elsewhere (Wong and Vecchio 2002).

Omitted in the analyses were models for dowel action, and bar buckling. Dowel action refers to the shear resistance provided by the reinforcing bars as the crack slips transversely to the axis of the reinforcement. This phenomenon requires calculation of slip deformations through the DSFM. Notably omitted was the consideration of bar buckling, which requires modeling the reinforcement as discrete elements and introduces complexity, albeit not overly difficult to implement, in the finite-element model. In keeping with the objectives of formulating simple finite-element models, all reinforcement was modeled as smeared, which explicitly assumes that the reinforcement and concrete are perfectly bonded and that bar buckling is not taken into account. This is not to suggest that bar buckling is not important, and in fact, wall tests have demonstrated that buckling may precede failure (Oesterle et al. 1976). However, the results of this study illustrate that assuming perfect bond between the concrete and the reinforcement still provides satisfactory results.

Material Properties

The finite-element method can require a significant amount of information regarding the material properties of the concrete and the reinforcement, which can affect the simulated behavior. For the design office engineer, this can pose a challenge. Typically, only the concrete compressive strength and the yield strength of the reinforcement are known at the onset; however, additional information would be required to describe the stress-strain responses for both materials. To simplify the analysis process, VecTor2 solely requires the cylinder compressive strength for the concrete material; the remaining properties are calculated internally (Wong and Vecchio 2002). For the reinforcement, the program requires information to construct a trilinear stress-strain response that includes the linear elastic region, the yield region, and the strain-hardening zone. For typical reinforcement grades, material properties such as Young's modulus, ultimate strength, the strain at strain hardening and the ultimate strain can be obtained from the literature or from past mill reports.

Slender Shear Walls

The first category of structural walls investigated is the slender shear wall, commonly viewed as having a wall height-to-width ratio greater than 2. The focus herein is the Portland Cement Association (PCA) structural walls (Oesterle et al. 1976), which are widely regarded as benchmarks against which theoretical formulations are corroborated against.

Results of a rectangular Wall (R1) and a flanged Wall (F1) are presented. Results of other PCA walls are provided in Table 1. Fig. 1 illustrates geometric details for the two types of walls investigated. In formulating a suitable finite-element mesh, the first task is to determine the number of distinct modeling "zones" in the structure. Changes in geometry and/or material properties, including changes in reinforcement ratio, necessitate new zones in the model. As indicated by the material properties listed in Table 2 and the geometric details in Fig. 1, the PCA walls required three distinct zones. Each wall was constructed with a uniform concrete strength; however, changes in the thickness and quantity of reinforcement in the boundary elements necessitated modeling of multiple zones. The rectangular Wall R1 contained distributed horizontal and vertical reinforcement in the center of the wall. This area was defined by one zone. In addition, concentrated reinforcement was placed at each end of the wall, which necessitated a second zone. Finally, the top and bottom slabs were stiff elements of similar thickness and constituted a third zone in the model. As a result Wall R1 was modeled with three zones.

Wall F1 was constructed with boundary flange elements. The central web wall, which contained distributed horizontal and vertical reinforcement, was modeled as a single zone. The boundary elements introduced a change in the thickness relative to the central web wall and contained concentrated vertical reinforcement, thus were modeled as a separate zone. Finally, the top and bottom slabs were modeled as stiff elements requiring a third zone.

After establishing the zones and the respective material properties, the user must develop a finite-element mesh that will be sufficient to capture the salient features of the structural behavior. In a situation where the user has prior knowledge of the test results, this process can be eased by continual refinement of the mesh until analytical results are satisfactory. For the practicing engineer who must design or analyze a structure without precise prior knowledge of behavior, mesh refinement is also recommended. An acceptable approach would be a mesh refinement study to verify that global displacements and local stresses do not change substantially, within tolerances required for design (5–10%), if the number of elements used in the mesh is doubled.

This study indicates that selecting 14–16 rectangular elements in the short direction of the wall, and aiming for an aspect ratio less than 1.5, unless there are constraints in the geometry of the structure that necessitate a larger aspect ratio, provides close agreement with test results. (Note that the 14- to 16-element suggestion is employed for the entire wall section including the boundary elements.) This approach usually suffices and is an acceptable starting point for design engineers and inexperienced FE analysts when conducting a mesh refinement study.

The elements employed in the analyses are low powered and are based on a linear displacement field (constant strain elements)

Table 1. Observed and Calculated Behaviors

	Lateral load (kN)			Lateral displacement (mm)			Failure mode	
Wall	Analytical	Experiment	Ana./expt.	Analytical	Experimental	Ana./expt.	Experimental	Analytical
R1	110	118	0.932	102	51	2.000	Bar buckling	Web crushing
F1	826	836	0.988	102	102	1.000	Web crushing	Web crushing
B1	263	271	0.970	152	102	1.490	Bar buckling	Web crushing
B2	682	704	0.969	127	102	1.245	Web crushing	Web crushing
B3	268	276	0.971	204	152	1.342	Bar fracture/bar buckling	Web crushing
B5	714	762	0.937	127	127	1.000	Web crushing	Web crushing
B6	815	825	0.988	76	76	1.000	Web crushing	Web crushing
B7	1010	980	1.031	152	127	1.197	Web crushing	Web crushing
B8	999	978	1.021	152	127	1.197	Web crushing	Web crushing
SW4	105	104	1.010	20	10	2.000	Crushing of boundary zone	Crushing of boundary zone
SW5	125	117	1.068	10	10	1.000	Diagonal tension/compression	Diagonal tension/compression
SW6	104	108	0.963	8	16	0.500	Diagonal tension	Crushing of boundary zone
SW7	128	127	1.008	10	18	0.556	Diagonal tension	Crushing of boundary zone
SW8	104	95	1.095	20	22	0.909	Crushing of boundary zone	Crushing of boundary zone
SW9	108	98	1.102	26	22	1.182	Web crushing	Web crushing
O1	526	575	0.915	5	5	1.000	Crushing of boundary zone	Crushing of boundary zone
O2	722	690	1.046	1.6	3.2	0.500	Sliding shear	Sliding shear
O7	422	380	1.111	10	10	1.000	Crushing of boundary zone	Crushing of boundary zone
O8	246	225	1.093	15	15	1.000	Crushing of boundary zone	Crushing of boundary zone
DP1	1296	1298	0.998	10	11	0.909	Widespread web crushing	Widespread web crushing
RW3	149	163	0.914	2.00%	2.50%	0.800	Crushing of column boundary zone	Crushing of column boundary zone
Mean			1.006			1.087		
COV (%)			6.1			36.4		

and the 14- to 16-element suggestion provides a relatively fine mesh to ensure the strain field assumption is valid. Finally, the top and bottom slabs are discretized to maintain continuity with the finite-element mesh developed for wall portion of the structure. Fig. 2 illustrates the finite-element models developed for Walls R1 and F1, respectively. In the end boundary zones the 1.5 aspect ratio is exceeded. The process in developing the model consisted of using 15 elements in the short direction (horizontal length for Wall R1). Each boundary zone was modeled with two of the initial 15 elements, and the central web wall contained the remaining 11 elements. One element in the boundary zone may not be sufficient to capture the salient features of behavior in this region, and the author consistently uses a minimum of two elements in each boundary zone. The height of the elements was based on maintaining an aspect ratio of not greater than 1.5 for the web elements. Consequentially, the elements in the boundary zone slightly exceeded the aspect ratio limit but not to the extent that the results are adversely affected.

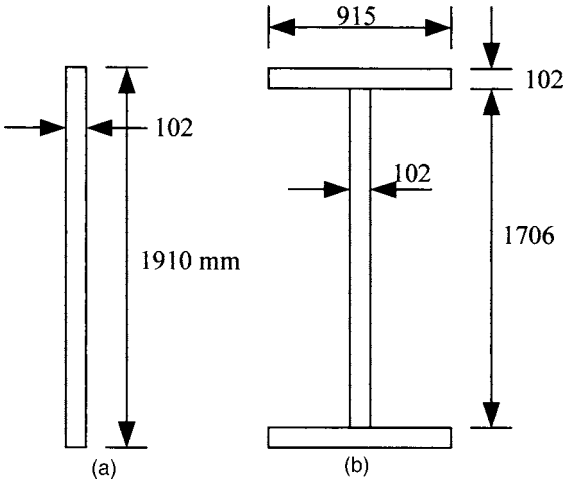

Fig. 1. Details of PCA walls: (a) Wall R1; (b) Wall F1

Development of a two-dimensional model for a structure with boundary elements, such as flanges, requires consideration of the effectiveness of the boundary element width in contributing to the lateral load resistance of the wall. Two-dimensional analyses assume the flange elements are fully connected to the web elements. Concentrating the full width of the flanges into a single element overestimates the degree of lateral and vertical confinement provided to the central web wall. Further, the shear lag that occurs in the out-of-plane direction cannot be considered. In addition, the ability of the flange elements in resisting lateral shear is overstated. These factors can lead to a response that overestimates the strength and stiffness of the wall relative to a three-dimensional model. The FE analyst could, in the case of a wide flanged wall, opt for a three-dimensional analysis. However, such an analysis places great demand on computational time, and this is significantly magnified in the case of reverse cyclic loading, which may not be economically justified in a design office. Recent North American codes, including the American Concrete Institute (ACI 2005) and the Canadian Standards Association (CSA 2004) have increased the effective overhanging flange width to 25% of the total wall height above the section under consideration. Considering Wall F1, which has an overhanging wall width of approximately 9% of the wall height, it appears reasonable to include the full width of the wall in the two-dimensional (2D) model. Wall

Table 2. Material Properties of PCA, SW4, O1, and DP1 Wall Specimens

			Reinforcement					
			Horizontal		Vertical		Confining	
Wall	Zone	Concrete f_c (MPa)	ρ (%)	f_y (MPa)	ρ (%)	f_y (MPa)	ρ (%)	f_y (MPa)
R1	Web	44.8	0.31	532	0.25	532		
	Boundary	44.8	0.31	532	1.47	512		
F1	Web	38.4	0.71	532	0.30	532		
	Boundary	38.4	0.71	532	3.89	445		
SW4	Web	37.0	0.39	545	0.50	545	—	—
	Boundary	37.0	1.18	545	6.86	470	0.43	545
O1	Web	25.0	0.26	425	0.57	435	—	—
	Boundary	25.0	1.00	425	1.33	435	0.27	425
DP1	Web	21.7	0.74	605	0.79	605		
	Boundary	21.7	0.58	605	0.63/0.23[a]	605		

[a]0.23% represents reinforcement near flange tips.

DP1 was constructed with overhanging flanges exceeding the prescribed code values and is further discussed in the section on squat walls.

Other modeling details that were consistent in the analyses included fully fixed base slabs and loading applied to the rigid top slab. The one exception was Wall RW3, which did not contain a top slab, therefore loading was introduced at the top of the central web wall. The loading regime in the analyses was consistent with laboratory conditions.

Figs. 3 and 4 provide the simulated and observed load-deformation responses of Walls R1 and F1, respectively. It is apparent that the simulated behaviors provide excellent agreement with the observed behaviors, while preserving the concept of simple modeling techniques. The ultimate load, energy dissipation, postpeak response, and failure mechanisms are well simulated. Details are provided in Table 1. The results indicate a discrepancy between the observed and predicted failure mode for R1. It was observed that bar buckling preceded failure, whereas the analysis predicted web crushing at the onset of failure. It is important to note that crushing of the concrete will generally occur as bars buckle in compression. By neglecting bar buckling, the predicted behavior predicts stiffer reloading responses during the second and third repetitions of loading. A closer examination of the predicted displaced shape of R1 reveals significant shear distortion in the lower portion of the wall. This phenomenon was also predicted for Walls B1 and B3, which also experienced bar buckling. The experimental observations indicated that significant shear distortion followed bar buckling. This suggests that although bar buckling was not explicitly modeled, the failure

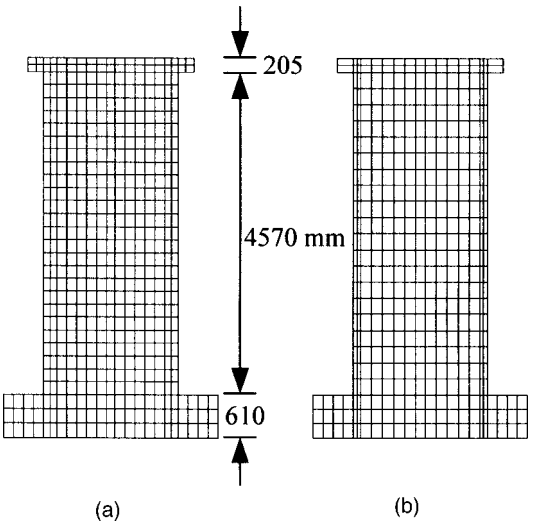

Fig. 2. Finite-element model of PCA walls: (a) Wall R1; (b) Wall F1

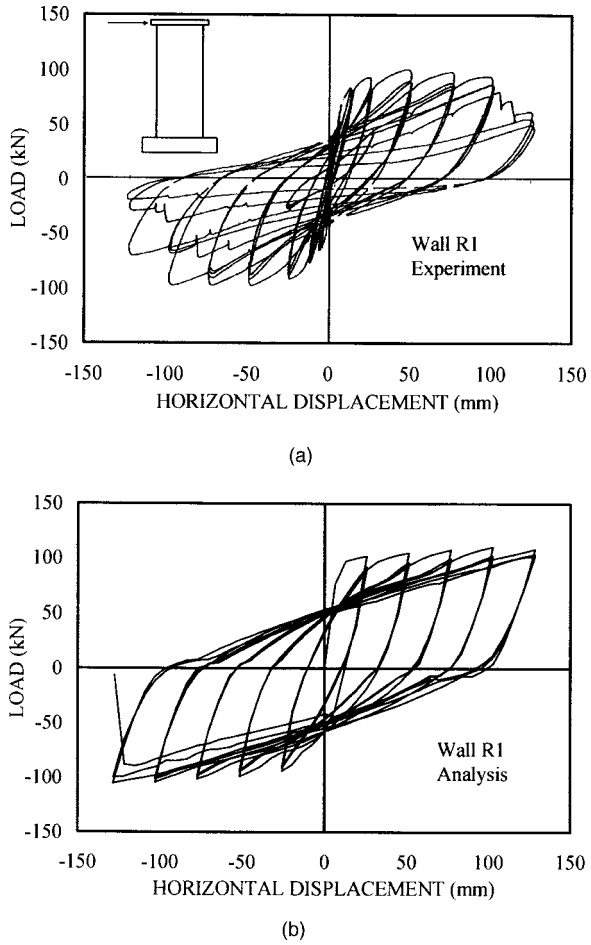

Fig. 3. Load-deformation responses of R1: (a) observed; (b) calculated

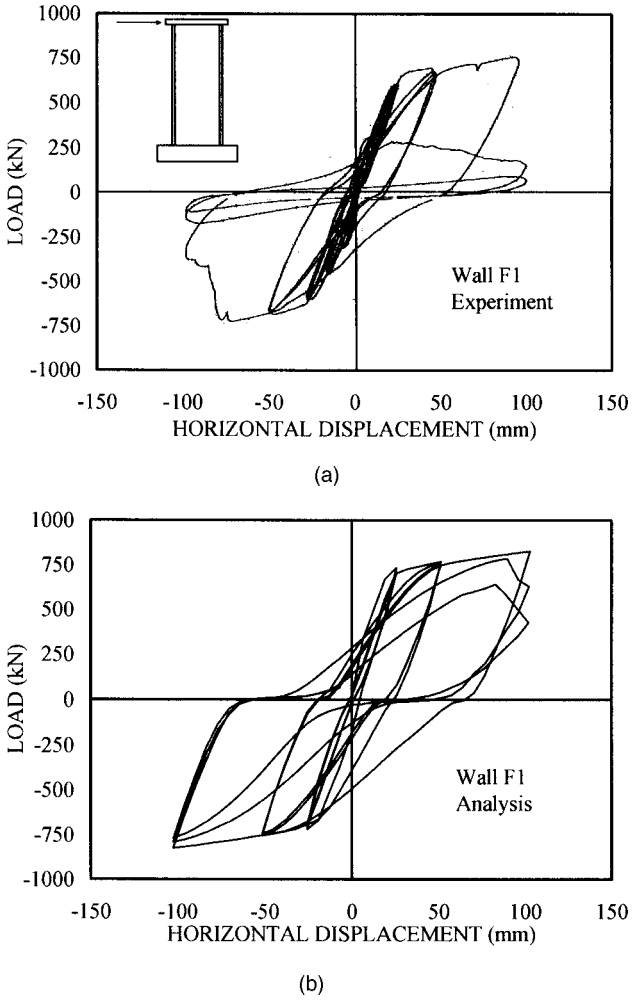

Fig. 4. Load-deformation responses of F1: (a) observed; (b) calculated

mechanism is consistent with the effects of bar buckling. The results listed in Table 1 further reveal that the peak lateral load is generally predicted with greater accuracy than the displacement corresponding to the peak lateral load. Specifically, Wall R1 demonstrates a greater discrepancy. The maximum lateral resistance was predicted at a displacement of 102 mm, whereas a displacement of 51 mm was the recorded during testing. A closer examination of the response reveals that this is actually a subtlety in behavior. The analysis predicted a maximum load of 110 kN at 102 mm, and a load of 105 kN at 52 mm. The observed behavior also demonstrates a marginal difference in lateral load for this range of displacements. This type of discrepancy should be expected for near flat-top responses, where the difference in load for a significant range of displacements is minimal.

Slender/Squat Shear Walls

The second set of shear walls investigated is the SW series tested at Imperial College (Pilakoutas and Elnashai 1995). The walls were rectangular with concealed boundary columns at each end of the wall. The walls were constructed with a height-to-width ratio of 2, which according to wall classification borders between slender and squat. Walls SW4–SW9 were analyzed, with SW4 discussed in further detail. Table 2 provides details pertaining to the material properties used in the analysis. The wall contained concentrated flexural reinforcement at the ends of the wall, necessitating boundary zones consisting of two elements in the horizontal direction in the model. Dimensional details are provided in Fig. 5, and the finite-element model is illustrated in Fig. 6. The observed and predicted response of Wall SW4 is illustrated in Fig. 7. The wall is well simulated by the finite-element model. The flat-top response of SW4 is accurately captured, and indicates a response that is dominated by yielding of the flexural reinforcement prior to failure. Table 1 indicates a significant difference in the displacement corresponding to the maximum lateral load for SW4. The observed maximum load of 104 kN was recorded at 10 mm of displacement, whereas the analysis predicted a load of 105 kN at a corresponding displacement of 20 mm. A closer examination of the load-deformation response reveals that at 10 mm of lateral displacement the analysis calculated a load of 104 kN. Similar to Wall R1, the difference in load for a significant range of displacements is marginal and the behavior is properly simulated.

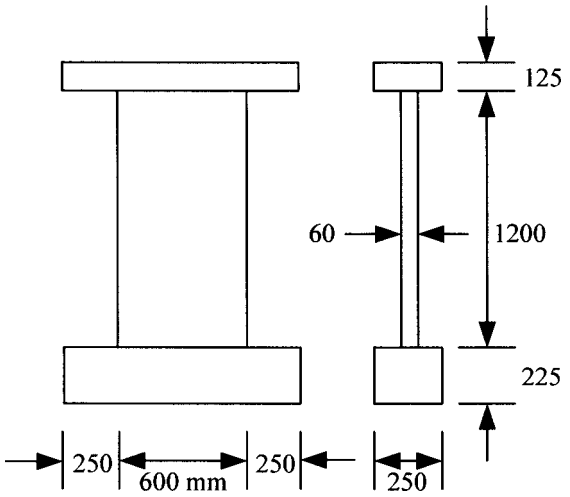

Fig. 5. Details of Wall SW4

Squat Shear Walls

The third set of walls investigated is the squat shear wall, which has a height-to-width ratio less than 2. The squat shear wall is typically integrated in the lateral load resisting mechanism of

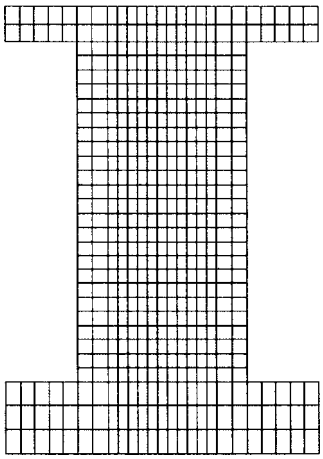

Fig. 6. Finite-element model of Wall SW4

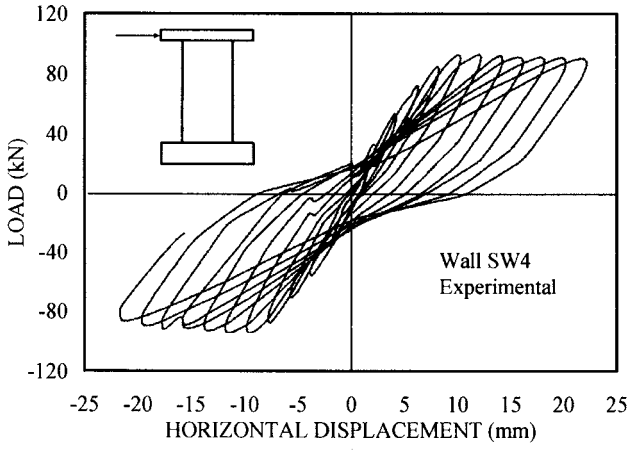

Fig. 7. Load-deformation responses of SW4: (a) observed; (b) calculated

low-rise buildings. The behavior of this classification of wall is heavily influenced by shear-related mechanisms, including pinched hysteresis loops, less energy dissipation relative to slender walls, and load-deformation curves that are more rounded and tend to resemble the base curve of concrete in compression. The geometry of squat walls promotes higher levels of shear stresses, leading to shear crushing of the concrete and possibly shear sliding along the base, providing a significant challenge to analysts. The sliding action prevents further increase in the lateral load carrying capacity. Generally, the near flat-top response associated with significant yielding of the flexural reinforcement observed in properly designed slender walls diminishes as the height-to-width ratio decreases. For squat walls, greater demand is placed on the concrete, which in turn provides a significant challenge to the concrete constitutive relationships employed during the analysis.

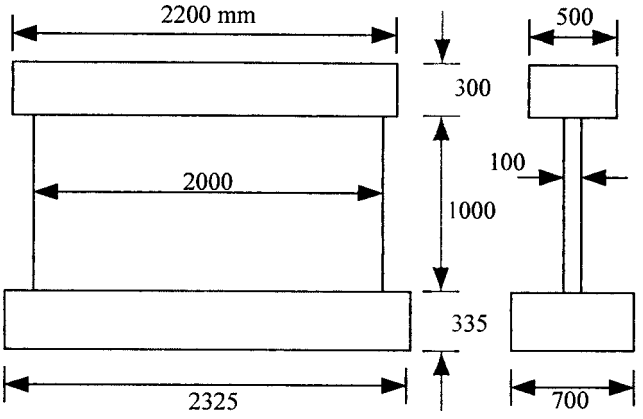

Fig. 8. Details of Wall O1

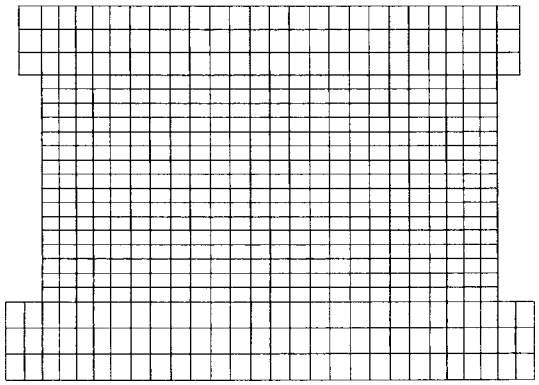

Fig. 9. Finite-element model of Wall O1

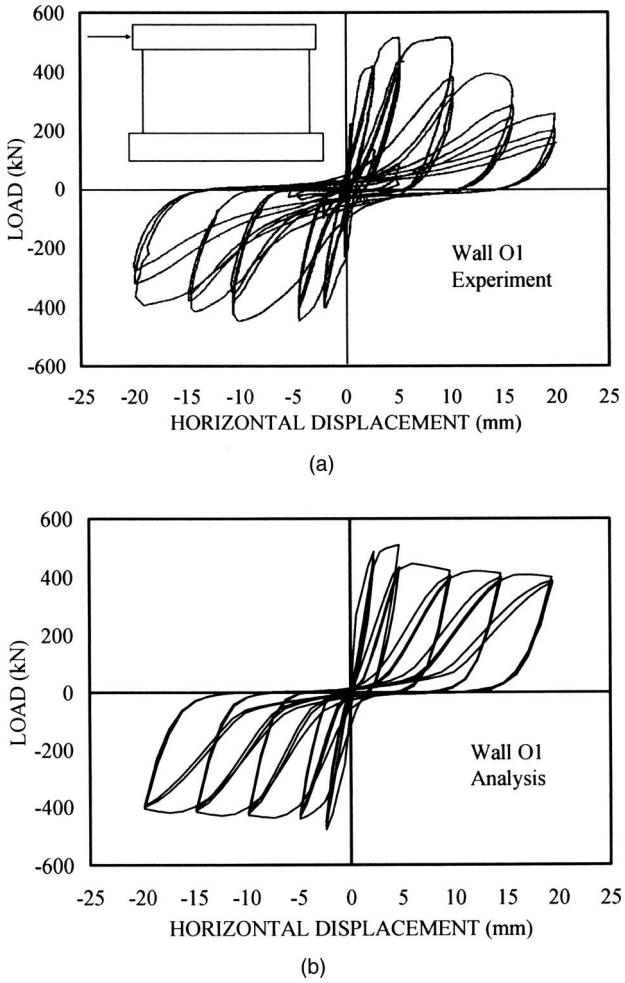

Fig. 10. Load-deformation responses of O1: (a) observed; (b) calculated

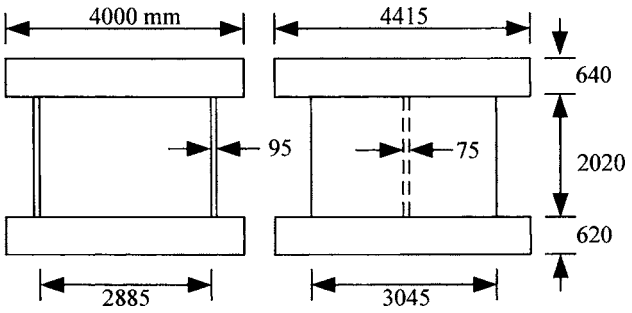

Fig. 11. Details of Wall DP1

The first group of walls analyzed are the O series tested at the University of Ottawa, specifically Wall O1 (Wiradinata and Saatcioglu 2002). The wall had a height-to-width ratio of 0.5 and was part of an experimental investigation to predict the behavior of squat walls.

Fig. 8 depicts the wall geometry and Fig. 9 illustrates the finite-element model for O1. The model contained four zones: one for the central portion of the wall, a second to model the concealed columns at each end of the wall, and two zones to model the top and base slab. Note that the 14- to 16-element suggestion was applied in the vertical direction (shortest dimension for Wall O1) and four elements were used in the boundary zones. Details of the material properties are provided in Table 2.

Fig. 10 describes the simulated and observed responses of Wall O1. It is evident that the analysis generally provides an accurate simulation of the load-deformation response. Other features that were successfully modeled include: peak lateral load, ductility, postpeak behavior, energy dissipation, and failure mode involving shear crushing of the compression toe. Discrepancies are subtle and include the rate of degradation in the postpeak regime. This can be attributed to the selection of the postpeak response for the concrete in compression.

Fig. 11 provides detail of Wall DP1 tested by Palermo and Vecchio (2002b). DP1 was part of an experimental investigation intended to provide data for developing improved constitutive modeling for concrete subjected to reverse loading. Table 2 provides information on the material properties for the concrete and the reinforcement.

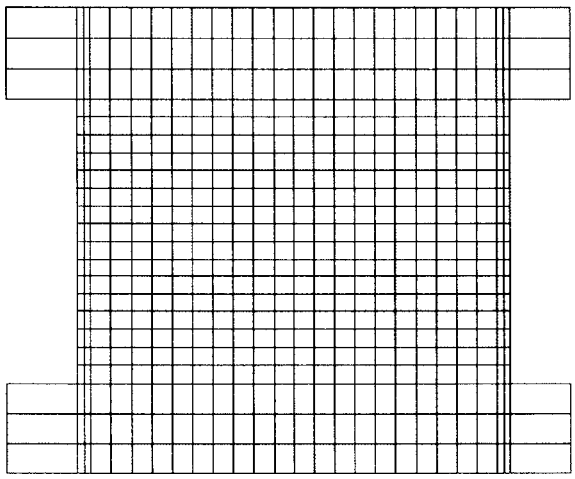

Fig. 12. Finite-element model of Wall DP1

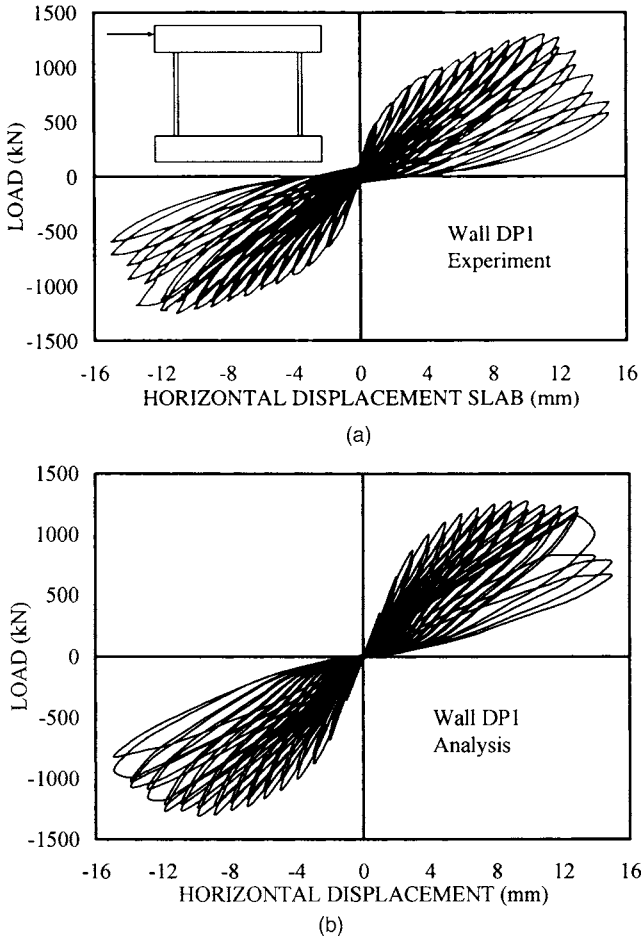

Fig. 13. Load-deformation responses of DP1: (a) observed; (b) calculated

The DP series of walls provide a formidable challenge for analysts. The walls are squat with the web elements experiencing heavy damage in the concrete during testing. Further complicating the analysis are the wide flanges at either end of the central web wall. The DP walls pose a greater challenge than other flanged walls available in the literature. The DP walls were constructed with overhanging flanges with an approximate width of 75% of the wall height; 50% larger than the prescribed effective overhanging flanges in current codes. The design standards provide a method to calculate the effective overhanging flange width when calculating the flexural strength, which has been traditionally based on a percentage of the wall height. In the case of a continuum finite-element analysis, flexural and shear strength calculations are not decoupled, and assuming an effective width based on flexure may not be representative of the shear stresses that are developed over the flanges. Vecchio (1998) conducted a parametric study on the effectiveness of flanges on the Nuclear Power and Engineering Corporation (NUPEC 1996) walls. The NUPEC walls are very similar to the DP series of walls. Vecchio observed that a flange width ranging between 67 and 100% was appropriate, resulting in an overhanging flange effectiveness between 48 and 72% of the wall height. It was further reported that decreasing the flange width promoted failure modes more heavily influenced by flexural mechanisms. A recent study of slender walls has suggested that the effective flange width is linked to the drift level (Hassan and El-Tawil 2003).

A parametric study of the effectiveness of the flanges for Wall

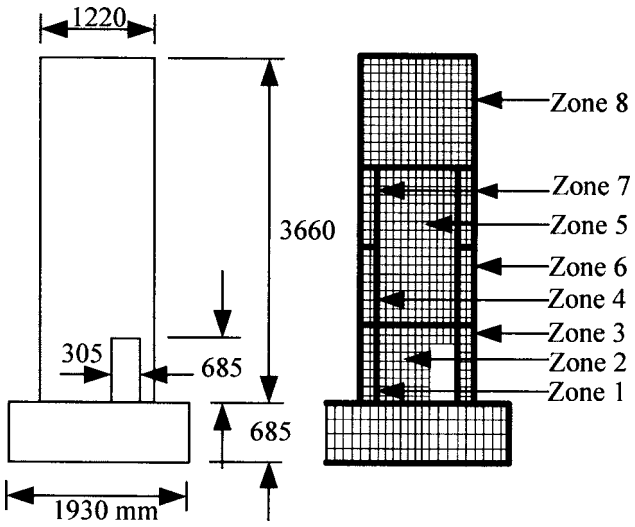

Fig. 14. Finite-element model of Wall RW3

DP1 was conducted. Two-dimensional analyses were performed considering flange widths ranging from 0 to 73.5% of the wall height. The latter representing the full width of the constructed specimen. The results reveal that a flange overhang of 50% of the wall height provides a close agreement in the prepeak range, while the full width of the flanges (73.5% overhang effectiveness) better represents the postpeak behavior. The 50% flange width effectiveness represents an increase of 100% relative to that prescribed by current codes, while the 73.5% effectiveness corresponds to a 194% increase. Based on these results DP1 was modeled with fully effective flange widths. Further research is required on the effectiveness of flanges, considering slender and squat walls including the effects of flexure and shear.

Wall DP1 was modeled with four zones, as shown in Fig. 12: the central web wall, the flanges, and the top and bottom slabs. The slabs were modeled separately to account for differences in concrete strength. Fig. 13 illustrates the experimental and analytical responses. The simulation provides substantial agreement with the observed response in all aspects of behavior: peak lateral load, energy dissipation, postpeak response, ductility, and failure mechanism. The simulation predicted a failure consistent with the observed behavior, which involved widespread damage to the concrete in the web wall in the form of equally spaced vertical crushing planes. The gradual softening in the postpeak regime was also accurately predicted.

DP1 failed by experiencing heavy damage to the concrete in the web elements. The flanges experienced flexural cracking; otherwise, no significant visual damage was evident. On examination of the data, the reinforcement in the flanges remained elastic on average; yielding was confined to crack locations. Similar results were predicted by the finite-element simulation. It appears that the flanges remained relatively stiff and the supposition of assigning the full width to be effective seems warranted.

Additional Analyses

An additional analysis was conducted on a shear wall typically encountered in design: a slender wall with openings. The openings can be representative of elevator doors or door openings leading to stairwells. Wall RW3 (Taylor, Cote, and Wallace 1998) was chosen for this study. The wall was part of an investigation to propose design procedures for slender walls with large openings in regions of significant inelastic deformations. Fig. 14 illustrates the geometry of Wall RW3.

The finite-element model for Wall RW3, shown in Fig. 14, required nine separate zones: eight to model the wall and one to model the rigid base foundation. Multiple wall zones were necessitated by the varying quantities of reinforcement along the wall height. Table 3 contains the material properties for each of the zones. The use of a preprocessor with an automatic mesh generator appreciably reduced the amount of time required to input the data and develop the model.

The experimental and analytical load-deformation responses shown in Fig. 15 indicate that the simulation accurately predicted the behavior capturing salient features, including the ultimate load, ductility, failure mechanism, and energy dissipation. The analysis accurately predicted the onset of failure, which included significant damage to the boundary zone nearest the opening in the wall. Table 1 also indicates that there was close agreement between the peak lateral load and the corresponding lateral drift.

Interpreting Results

Complexities involved in interpreting the results were one of the areas of concern in a recent criticism of the finite-element method (Orakcal et al. 2004). This criticism was reasonable when results of finite-element analyses were stored in large text files. Typical analyses containing hundreds of elements would result in a laborious task of sorting through extensive data on strains and stresses

Table 3. Material Properties of RW3 Wall

			Reinforcement					
			Horizontal		Vertical		Confining	
Wall	Zone	Concrete f_c (MPa)	ρ (%)	f_y (MPa)	ρ (%)	f_y (MPa)	ρ (%)	f_y (MPa)
Rw3	1	31	0.66	414	2.93	414	0.57	414
	2	31	0.66	414	0.50	414	—	—
	3	31	0.50	414	2.93	414	0.76	414
	4	31	0.33	414	2.93	414	0.57	414
	5	31	0.33	414	0.33	414	—	—
	6	31	0.33	414	2.93	414	0.76	414
	7	31	0.33	414	2.93	414	—	—
	8	31	3.00	414	3.00	414	—	—

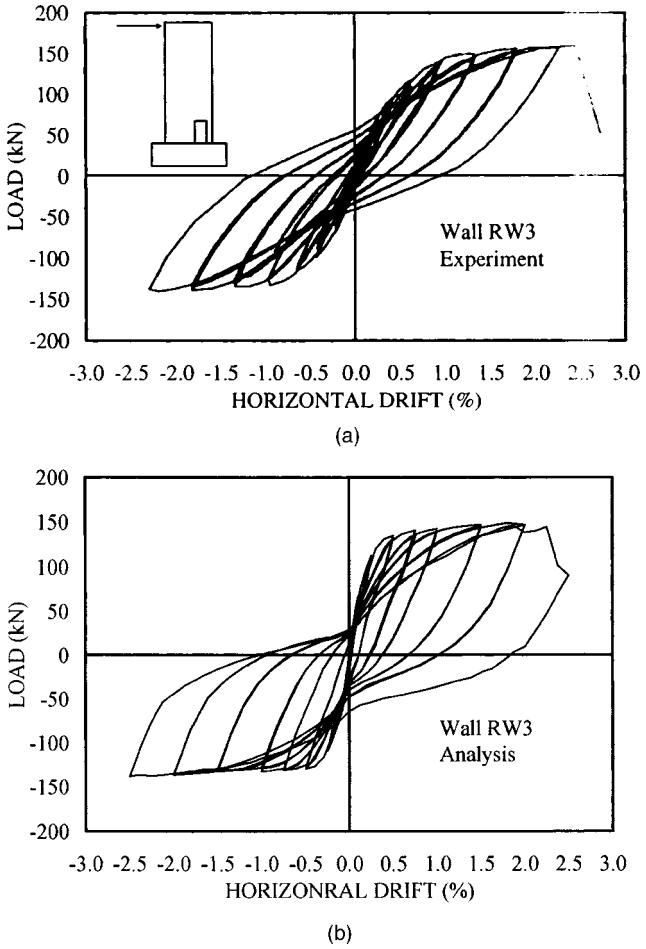

Fig. 15. Load-deformation responses of RW3: (a) observed; (b) calculated

for each element and each load stage. This task would be magnified when an analysis based on reverse cyclic loading is considered, where hundreds to thousands of load stages would be recorded. However, with tremendous strides in computational power and programming languages, the arduous task of sifting through data is alleviated with the aid of graphical and visual postprocessors.

The finite-element models in this study were developed using a graphical interface (Wong and Vecchio 2002) capable of generating finite-element models. The user is only required to input the four corners of each zone and to link the material properties to each zone. The user has the option of specifying the aspect ratio of the element to generate in each zone. The mesh is then generated and the user has a visual representation of the model, which can be refined until a satisfactory model is developed. After the analyses were complete the results were available through a postprocessor. (Most modern FE packages have useful graphics-based pre- and postprocessors.) Figs. 16(a and b), generated with the aid of a postprocessor, illustrate the displaced shape of Wall DP1 and the extent of concrete crushing, respectively. The shaded regions in the central web wall indicate the locations where concrete was significantly damaged. In this case the analyst has a visual representation of failure coinciding with crushing of the concrete in the web wall along five vertical bands. This is consistent with observations during testing (Palermo and Vecchio 2002b). The postprocessor uses a similar shading technique to display other results,

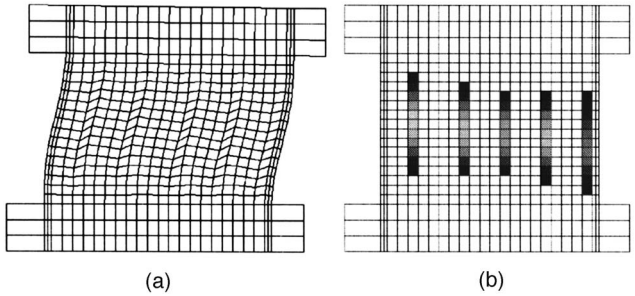

Fig. 16. Calculated failure mode of DP1: (a) displacements; (b) concrete crushing

including strains and stresses in the concrete and reinforcement, the percentage of concrete crushing or reinforcement yielding, and crack widths, among other pertinent information.

Conclusions

The analyses conducted in this paper on various shear walls ranging from slender to squat, including various cross sections commonly encountered in practice, have served to address recent criticism about the finite-element method's practicality, reliability, and robustness. Simple models capable of providing quick and reliable results were developed with the use of a preprocessor. This consisted of employing low-powered rectangular elements, and smearing of the material properties throughout the elements. Simple rules were suggested for mesh configuration and refinement: utilizing 14–16 elements in the shortest direction and aiming for an aspect ratio of 1.5. Further discussions focused on the effective width of boundary elements for 2D analyses. For this study the boundary elements were assumed fully effective and this supposition did not adversely affect the simulated behaviors.

The analyses provided simulations that were in substantial agreement with the observed behaviors, including peak strength, postpeak response, ductility, energy dissipation, and failure mechanisms. The only noticeable discrepancy was related to the displacement corresponding to the peak lateral load. However, upon further investigation, the analyses of walls that seemed to suggest gross errors were not as noteworthy. Such walls demonstrated flat-top load-deformation responses and the degradation of the lateral load for a significant portion of the response was minimal, suggesting that the displacement corresponding to peak lateral load can lie within a range of displacements.

The results were examined using a postprocessor, eliminating the need to sort through vast quantities of data in text files for each load stage. The advent of visual and graphical pre- and postprocessors has also addressed the criticism that developing the finite-element model and interpreting results can be a convoluted experience with high potential for error.

In short, this study has brought to the fore the practicality, reliability, and possible simplicity of the finite-element method, while providing accurate simulations of structural behavior that can be incorporated into the design and analysis tools of practicing engineers.

References

American Concrete Institute (ACI). (2005). "Building code requirements for structural concrete and commentary." *ACI 318-05*, Farmington Hills, Mich.

ASCE (2001). "Modeling of inelastic behaviour of RC structures under seismic loads." *Proc., Publ. No. 0-7844-0553-0*, Reston, Va.

Canadian Standards Association (CSA). (2004). "Design of concrete structures." *CSA A23.3-04*, Mississauga, Ont.

Clough, R. W. (1980). "The finite element method after twenty-five years: A personal view." *Comput. Struct.*, 12(4), 361–370.

Cook, R. D. (1995). *Finite element modeling for stress analysis*, Wiley, New York.

Darwin, D., and Pecknold, D. A. (1976). "Analysis of RC panels under cyclic loading." *J. Struct. Div.*, 102(ST2), 355–369.

Foster, S. J., and Marti, P. (2003). "Cracked membrane model: FE implementation." *J. Struct. Eng.*, 124(12), 1155–1163.

Hassan, M., and El-Tawil, S. (2003). "Tension flange effective width in reinforced concrete shear walls." *ACI Struct. J.*, 100(3), 349–356.

Nuclear Power Engineering Corporation of Japan (NUPEC). (1996). "Comparison report, seismic shear wall ISP, NUPEC's seismic ultimate dynamic response test." *Rep. No. NU-SSWISP-D014*, Organization for Economic Co-Operation and Development, Paris.

Oesterle, R. G., Fiorato, A. E., Johal, L. S., Carpenter, J. E., Russell, H. G., and Corley, W. G. (1976). "Earthquake-resistant structural walls—Tests of isolated walls." *Rep. National Science Foundation*, Construction Technology Laboratories, Portland Cement Association, Skokie, Ill.

Okamura, H., and Maekawa, K. (1991). *Nonlinear analysis and constitutive models of reinforced concrete*, Giho-do Press, Univ. of Tokyo, Tokyo.

Orakcal, K., Wallace, J. W., and Conte, J. P. (2004). "Nonlinear modeling and analysis of slender reinforced concrete walls." *ACI Struct. J.*, 101(5), 688–698.

Palermo, D., and Vecchio, F. J. (2002a). "Behaviour and analysis of reinforced concrete walls subjected to reversed cyclic loading." *Rep. No. ISBN 0-7727-7553-2*, Dept. of Civil Engineering, Univ. of Toronto, Toronto.

Palermo, D., and Vecchio, F. J. (2002b). "Behaviour of three-dimensional reinforced concrete shear walls." *ACI Struct. J.*, 99(1), 81–89.

Palermo, D., and Vecchio, F. J. (2003). "Compression field modeling of reinforced concrete subjected to reverse loading: Formulation." *ACI Struct. J.*, 100(5), 616–625.

Palermo, D., and Vecchio, F. J. (2004). "Compression field modeling of reinforced concrete subjected to reverse loading: Verification." *ACI Struct. J.*, 101(2), 155–164.

Pilakoutas, K., and Elnashai, A. (1995). "Cyclic behaviour of reinforced concrete cantilever walls. Part I: Experimental results." *ACI Struct. J.*, 92(3), 271–281.

Sittipunt, W., and Wood, S. L. (1995). "Influence of web reinforcement on the cyclic response of structural walls." *ACI Struct. J.*, 92(6), 745–756.

Taylor, C. P., Cote, P. A., and Wallace, J. W. (1998). "Design of slender reinforced concrete walls with openings." *ACI Struct. J.*, 95(4), 420–433.

Vecchio, F. J. (1989). "Nonlinear finite element analysis of reinforced concrete membranes." *ACI Struct. J.*, 86(1), 26–35.

Vecchio, F. J. (1992). "Finite element modeling of concrete expansion and confinement." *J. Struct. Eng.*, 118(9), 2390–2406.

Vecchio, F. J. (1998). "Lessons learned from the analysis of a 3-D concrete shear wall." *Struct. Eng. Mech.*, 6(4), 439–455.

Vecchio, F. J. (1999). "Towards cyclic load modeling of reinforced concrete." *ACI Struct. J.*, 96(2), 193–202.

Vecchio, F. J. (2000). "Disturbed stress field model for reinforced concrete: Formulation." *J. Struct. Eng.*, 126(9), 1070–1077.

Vecchio, F. J., and Bucci, F. (1999). "Analysis of repaired reinforced concrete structures." *J. Struct. Eng.*, 125(6), 644–652.

Vecchio, F. J., and Collins, M. P. (1986). "The modified compression field theory for reinforced concrete elements subjected to shear." *J. Am. Concr. Inst.*, 83(2), 219–231.

Vecchio, F. J., and Collins, M. P. (1993). "Compression response of cracked reinforced concrete." *J. Struct. Eng.*, 119(12), 3590–3610.

Vecchio, F. J., Lai, D., Shim, W., and Ng, J. (2001). "Disturbed stress field model for reinforced concrete: Validation." *J. Struct. Eng.*, 127(4), 350–358.

Wiradinata, S., and Saatcioglu, M. (2002). "Behaviour of squat walls subjected to load reversals." *Publication No. OCCERC 02-25*, The Joint Centre of the Univ. of Ottawa and Carelton Univ., Ottawa.

Wong, P. S., and Vecchio, F. J. (2002). "*VecTor2* and *Formworks* user's manual." *Rep.*, Civil Engineering, Univ. of Toronto, Toronto.

Wong, S. Y., and Vecchio, F. J. (2003). "Towards modeling of reinforced concrete members with externally bonded fiber-reinforced polymer composites." *ACI Struct. J.*, 100(1), 47–55.